

MÖSSBAUER AND MAGNETIC INVESTIGATION OF IRON NITRIDE WITH MARTENSITE STRUCTURE SYNTHESISED FROM OXY-HYDROXIDE TYPE PRECURSOR

P. PALADE*, C. PLAPCIANU, I. MERCIONIU, C. C. COMANESCU,
G. SCHINTEIE

*National Institute of Materials Physics, Magurele, Bucharest, P. O. Box MG-7,
077125, Romania*

Fe₁₆N₂ fine particles were prepared by reduction in 5% H₂/Ar gas mixture flow, starting from goethite or hematite precursors, followed by nitridation in ammonia gas flow. Small amounts of metallic iron and iron oxide are present besides the main phase which is an ordered iron nitride having martensite structure (α'' -Fe₁₆N₂) as revealed by Mössbauer spectroscopy measurements. However, X-ray diffraction data do not show any traces of oxides due to their high degree of amorphization. When nitridation is performed at about 150 °C, Fe₄N phase begins to form and its presence deteriorates the magnetic properties. The samples prepared by nitridation of goethite present better magnetic properties compared to those obtained by nitridation of hematite. Magnetic and Mössbauer measurements performed at ambient temperature were corroborated in order to extract the magnetization at saturation value for each phase which occurs in the obtained samples. The corresponding values are 226 emu/g for Fe₁₆N₂ and 198 emu/g for metallic iron contained in the prepared powders.

(Received November 11, 2015; Accepted January 11, 2016)

Keywords: Iron nitride; Martensite; Ammonia; Mössbauer spectroscopy; Hysteresis

1. Introduction

High performance and cheap permanent magnets are imperatively required due to the exponential increase of the demands for various applications and also considering the limited resources of rare earths. The search for rare earth-free magnets became feverish in the last years. One of the most promising rare-earth free compound with very good magnetic properties is the ordered phase α'' -Fe₁₆N₂ with martensite-type body-centered tetragonal structure obtained by insertion of nitrogen into the body-centered cubic structure of α -iron generating a distortion along the c-axis direction. This compound was firstly synthesized in bulk form by Jack [1] via a rapid quenching of austenite-type phase of iron nitride (γ -FeN) in order to obtain disordered α' -Fe₁₆N₂ phase and further subsequent long time annealing to get the ordered α'' -Fe₁₆N₂ phase. After annealing, besides martensite-type phase, it occurs still residual austenite nitride phase, about 50% even after treatment at 120 °C for three weeks. Fe₁₆N₂ deposited as thin film was first time produced in 1972 by Kim and Takahashi [2], and the experimental magnetic moment per atom was giant, 3 μ_B . This value is about 40% higher than that of pure metallic iron (2.2 μ_B). Data from literature show a relatively wide range of magnetic moment values for Fe₁₆N₂ thin films, between 2.4 – 3.4 μ_B per atom, obtained by: molecular beam epitaxy (MBE) [3], radio frequency sputtering [4] and ion implantation [5]. Wang et al. [6] found that Ti addition improves the thermal stability of thin films containing Fe₁₆N₂. Similar studies performed by Atiq et al. [7] show that Co also improves the thermal stability while Cr decreases strongly the magnetization at saturation. Tayal et al. [8] found that small addition of Zr or Ti improves the structural and magnetic stability of the thin films. Not only experimental, but also theoretical studies support a high value of the

*Corresponding author: palade@infim.ro

magnetization at saturation spanning from 2.3 μ_B [9] to 2.9 μ_B per atom [10]. By low – temperature nitridation (110 °C) of fine iron powder having 20 nm diameter [11] for 10 days it was possible to obtain $Fe_{16}N_2$ with high yield however, due to surface oxidation, the saturation magnetization was only 162 emu/g. Further on, the synthesis of $Fe_{16}N_2$ by low temperature nitridation was performed by Kikkawa et al. [12] who studied the influence of temperature on the $Fe_{16}N_2$ formation. The same group analyzed the effect of particle size on the $Fe_{16}N_2$ yield and found, for optimized preparation parameters, a saturation magnetization value at ambient temperature of about 225 emu/g [13]. The humidity effects during preparation of $Fe_{16}N_2$ were studied by Yamanaka et al. [14] and the crystal structure of α ''- $Fe_{16}N_2$ phase was refined by Yamashita et al. [15]. It has been found by Masubuchi et al. that Co addition enhances the soft-magnetic properties of α ''- $Fe_{16}N_2$ particles obtained by low temperature nitridation [16]. By hydroxyapatite coating of iron nitride particles Nagai et al. [17] obtained an enhancement of coercivity of the fine particles. Takagi et al. [18] prepared a sintered magnet based on $Fe_{16}N_2$ fine particles. The high value of the saturation magnetization of $Fe_{16}N_2$ is useful for medical applications such targeted drug delivery [19] and hyperthermia [20]. The efficiency of low temperature nitridation processes as well as the coercivity and saturation magnetization for the final $Fe_{16}N_2$ product depends not only on temperature, reaction time and precursor particle dimensions used for nitride synthesis, but also on the morphology, type of oxide/oxy-hydroxide precursor, porosity and method of precursor preparation. The aim of the present work is to study the preparation of $Fe_{16}N_2$ from goethite precursor and to analyze in detail the influence of preparation parameters on the magnetic properties of the desired nitride. We chose the goethite precursor taking into account that the anisotropy shape of the acicular particle of goethite could increase the coercivity of the obtained $Fe_{16}N_2$ particles, while maintaining a high value of the saturation magnetization.

2. Experimental

The goethite precursor used for the preparation of $Fe_{16}N_2$ fine particles was prepared from $Fe(NO_3)_3 \cdot 9H_2O$ and KOH (Alfa Aesar, 99% purity). The amounts of 50 ml of 1M $Fe(NO_3)_3 \cdot 9H_2O$ and 90 ml 5M KOH aqueous solutions were mixed together and diluted in 1 L of deionized water and closed in polypropylene bottle. The precipitate of ferrihydrite formed immediately after mixing was kept for 100 h at 70 °C in order to obtain fine particles of goethite with acicular shape. The precipitate was separated from supernatant by filtration and it was washed several times until neutral pH. Next, the precipitate was dried using a drying stove. The oxy-hydroxide goethite precursor was then reduced at 450 °C for 10 h under 5% H_2 + 95% Ar (5.0 purity) flow using a tubular furnace. After cooling down, without taking out the powder from the furnace, the gas was switched to ammonia (5.0 purity) and the particles were treated for another 48 h in ammonia gas flow at 140°C and higher temperatures. Finally, the particles were cooled to room temperature and purged with nitrogen gas. Powder X-ray diffraction measurements were performed using a Bruker D8 Advance diffractometer with Cu $K\alpha$ radiation for the identifications of various phases in the studied materials. The morphology of the particles was investigated using a Lyra-Tescan SEM apparatus. The phase composition and the local magnetic interactions of iron containing materials were analyzed by Mössbauer Spectroscopy using a Co^{57} radioactive source and an integrated system (SEECO) operating under constant acceleration mode. The Mössbauer spectra were decomposed in spectral components and analyzed with the NORMOS program. Hysteresis loops at 300 K were acquired using a SQUID magnetometer (Quantum Design) running under the RSO (Reciprocating Sample Option) mode.

3. Results and discussion

As shown in the XRD pattern from Fig. 1A the oxy-hydroxide precursor obtained by the preparation method described in Experimental section is pure goethite (JCPDS file 29-0713) with relatively sharp peaks without indication of any amorphous contribution. After reduction in 5% H_2

+ 95% Ar (5.0 purity) flow for 10 h at 450 °C, the goethite was completely transformed into metallic iron (Fig. 1B). The peaks of metallic iron are very sharp indicating a high degree of crystallinity. Another preparation method implies as first step the conversion of goethite (α -FeOOH) into hematite (α -Fe₂O₃) by heating the goethite precursor in air for 4 h at 400 °C. The Fe₁₆N₂ fine particles can be prepared as well from goethite precursor and from hematite precursor, following the same preparation method: 10h at 450 °C in 5% H₂ + 95% Ar (5.0 purity) gas flow, followed by 48 h at 140 °C or higher temperatures in NH₃ (5.0 purity) gas flow. Fig. 2 presents the XRD patterns belonging to goethite or hematite reduced in 5% H₂/Ar gas flow in the first step and, in the second step, thermally treated in ammonia gas flow at lower temperature for 48 h. The samples, as presented in Fig. 2, are: (i) S1 – starting from goethite precursor and heated in ammonia gas flow (nitrided) at 140 °C, (ii) S2 – starting from hematite precursor and nitrided at 140 °C, (iii) S3-starting from goethite precursor and nitrided at 150°C, (iv) S4-starting from goethite crushed in mortar and processed in ultrasonic bath and afterwards nitrided at 140 °C. For all samples, the main phase obtained during preparation process was Fe₁₆N₂. As specified in the 78-1865 JCPDS file, which belongs to this phase, the two most intense peaks are located at $2\Theta = 42.698^\circ$ (corresponding to the reflection (202)) and $2\Theta = 44.778^\circ$ (reflection (220)). For pure Fe₁₆N₂ the intensity ratio between the (202) and (220) reflections must be about 2. The deviation from this ratio is caused by the presence of some other impurity phase. For all samples, besides Fe₁₆N₂ main phase, various amount of metallic iron can be observed. For sample S1 the amount of metallic iron is the lowest among all samples (below 10%). Additionally, for sample S3 it can be observed some contribution belonging to Fe₄N phase with broad peaks, indicating small crystallites with highly distorted structure. There is no evidence of any trace of oxides in all samples. Anticipating, according to Mössbauer data, all the samples contain iron (III) oxides, but they can't be detected in XRD patterns. The explanation could be that iron oxides occur in the samples as very small particles or shells with highly distorted structure for the cores belonging to particles of metallic iron or iron nitride. In our case the (220) reflection from Fe₁₆N₂ overlaps with the most intense reflection of metallic iron (110) at $2\Theta = 44.675^\circ$. Consequently, a rough estimation of the ratio between Fe₁₆N₂ and metallic Fe is the ratio between the area of the most intense two peaks of the diffractograms from Fig. 2 (at about $2\Theta = 42.7^\circ$ and $2\Theta = 44.7^\circ$, respectively). The ratio varies from 2 for pure Fe₁₆N₂ to 0 for pure metallic iron and this parameter is important in order to see the efficiency of the nitridation process, i.e. of the conversion of metallic iron into Fe₁₆N₂. A rough estimation of the ratio between the amount of Fe₁₆N₂ and bcc Fe from samples can be done using also the ratio between the weighted areas of the peaks belonging to the (422) reflection for Fe₁₆N₂ ($2\Theta = 81.106^\circ$) and (211) reflection for metallic iron ($2\Theta = 82.335^\circ$). The weighted areas are required because on a 100% scale for bcc Fe the intensity of (211) reflection of metallic iron is about 30% while on a 100% scale for Fe₁₆N₂ the intensity of (422) reflection of Fe₁₆N₂ is about 15%. In this second case the peaks are relatively well separated and not overlapping as for (220) reflection from Fe₁₆N₂ and (110) reflection from bcc Fe and allow a good estimation of the ratio between Fe₁₆N₂ and bcc Fe amounts which is presented in Table 2 together with the same estimation using Mössbauer data on samples S1, S2, S3, S4.

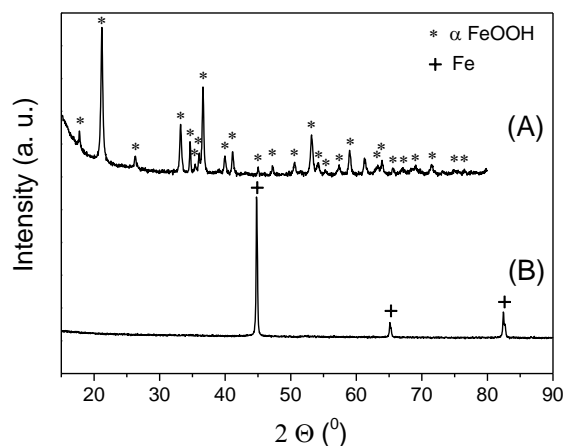


Fig. 1. X-ray diffraction patterns of as prepared goethite (A) and metallic iron (B) obtained from goethite by reduction in H_2/Ar mixture at $450^\circ C$

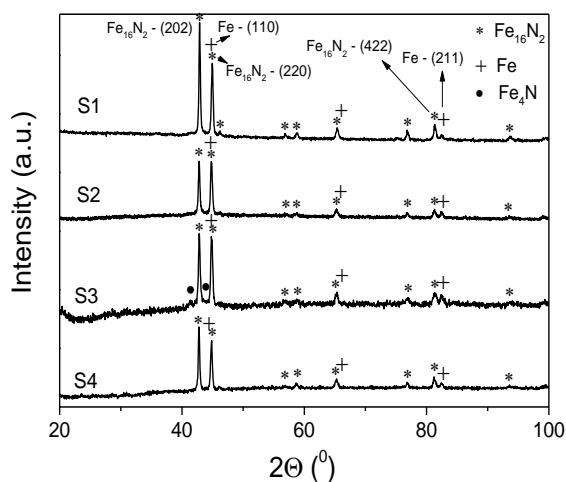


Fig. 2. X-ray diffraction patterns of samples: (i) S1 – starting from goethite precursor and heated in ammonia gas flow (nitrided) at $140^\circ C$, (ii) S2 – starting from hematite precursor and nitrided at $140^\circ C$, (iii) S3 – starting from goethite precursor and nitrided at $150^\circ C$, (iv) S4 – starting from goethite crushed in mortar and processed in ultrasonic bath and nitrided at $140^\circ C$.

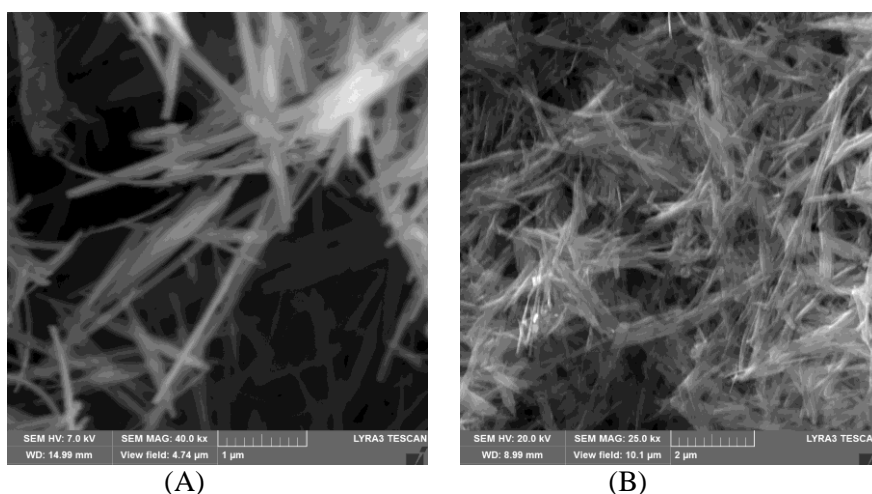


Fig. 3. SEM images of as prepared goethite (A) and hematite (B) obtained by heating the goethite in air at $400^\circ C$

Fig. 3 shows the SEM pictures for as prepared goethite (Fig. 3A) and for hematite obtained by heating goethite in air (Fig. 3B). The morphology of goethite is acicular and the particles have diameters of 100 nm or less and lengths of 2000 nm or more. After heat treatment in air of the goethite, the acicular particles (in this case of hematite) maintain their acicular form and dimensions as before heat treatment but they start to agglomerate and possibly also to stick together in some regions.

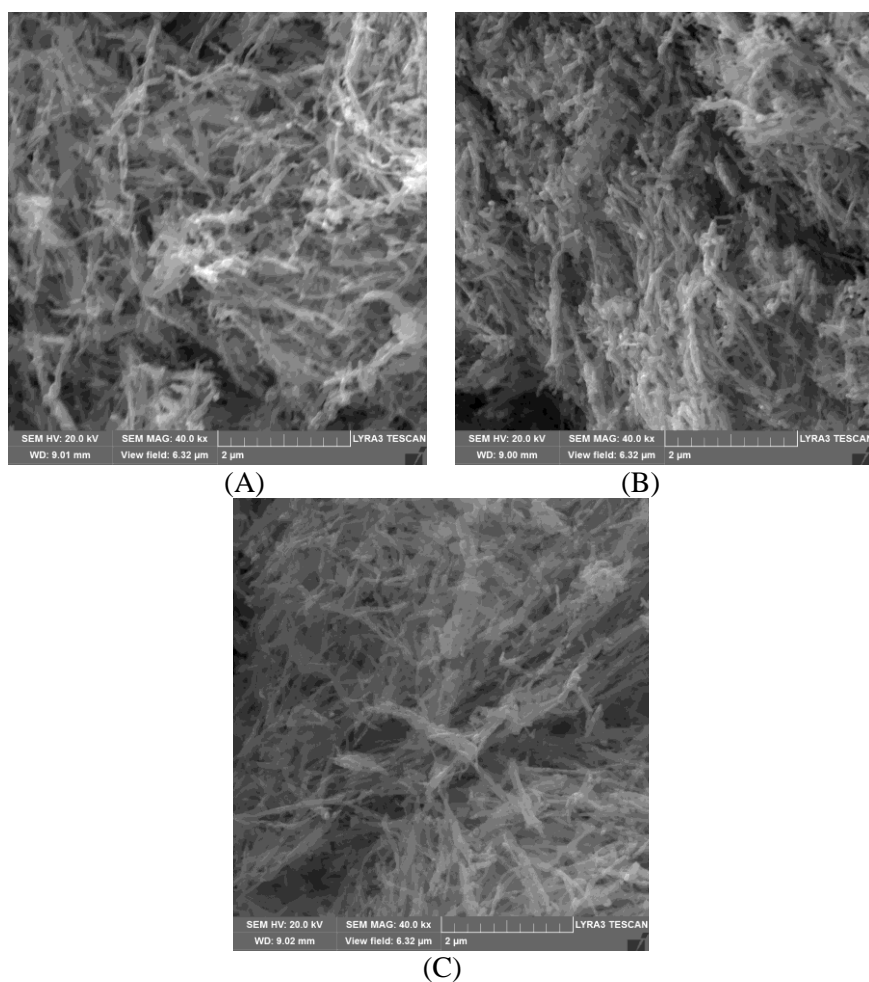


Fig. 4. SEM images of goethite nitrided at 140^oC (sample S1) - (A), hematite nitrided at 140^oC (sample S2) - (B) and goethite nitrided at 150^oC (sample S3) –(C)

Fig. 4 presents the SEM images for samples S1 (Fig. 4A), S2 (Fig. 4B), S3 (Fig. 4C). Sample S1 obtained by nitridation of goethite at 140^oC preserves the acicular form of the goethite precursor, but the particles become smaller and have some nodes emerging from the main trunk of the particle. The particles in S1 are still well separated but they become shorter compared with those from as prepared goethite while the diameter remains more or less constant.

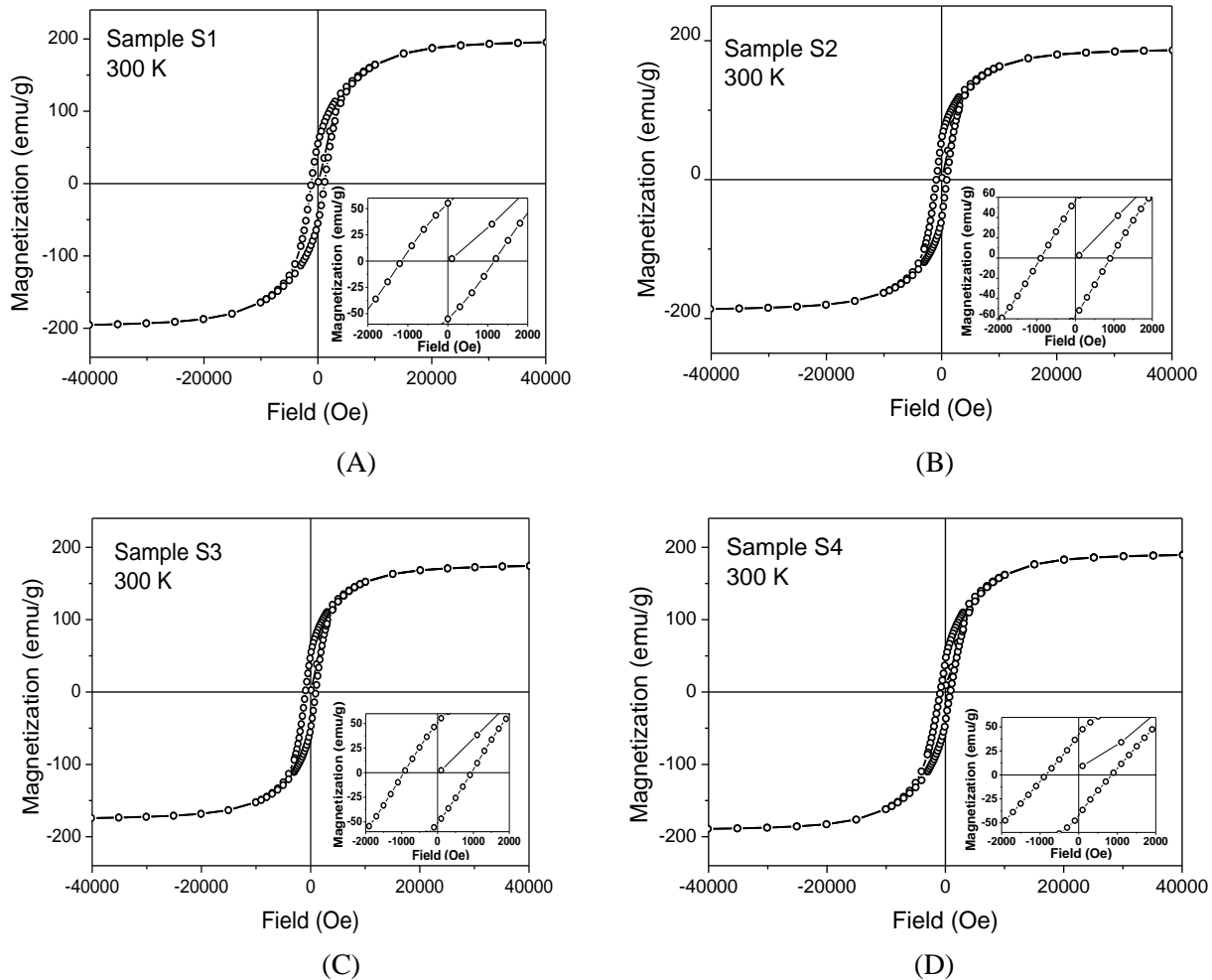


Fig. 5. Hysteresis loops at 300 K for samples: S1 – as prepared goethite nitrided at 140 °C, S2 - hematite nitrided at 140 °C, S3 – goethite nitrided at 150 °C, S4 – processed goethite nitrided at 140 °C (in the inset is shown the central part with high magnification)

Very important is the fact that even after reduction at 450 °C and long time heating in ammonia at 140 °C the particles do not stick together and maintain the shape anisotropy with good effect on the magnetic properties (especially high coercivity and remanence). Fig. 4C shows the SEM image of the goethite treated in ammonia gas flow at 150 °C (sample S3). Compared with the sample S1 (nitrided at 140 °C), for the sample S3 one may observe that acicular particles started to stick together. For the sample obtained from hematite precursor (sample S2), the structure is more compact (Fig. 4B) and even though the acicular shape is preserved to some extent, the particles begin to agglomerate and do not occur as dispersed as in the case of those obtained by nitridation of the goethite precursor. Comparing with the hematite precursor (Fig. 3B) the particles after nitridation at 140 °C of hematite (Fig. 4B) are shorter and present some regions where they are welded together. The idea which arises when analyzing all SEM information is that iron nitride obtained from the goethite precursor has a lower degree of agglomeration and sticking compared with the one obtained from the hematite precursor. The degree of sticking between particles increases by rising the temperature for the samples obtained from goethite precursor. The agglomeration of the particles is unfavorable for the penetration of ammonia during low temperature nitridation and consequently implies a low yield of iron transformation into iron nitride. On the other hand, the shortening and sticking of the particles could negatively influence the magnetic properties, diminishing the remanence and coercivity values.

Table 1. Magnetization at saturation, coercive field and remanence for samples S1, S2, S3, S4

Sample	Magnetization at saturation (M_s) (emu/g)	Coercive field (H_c) (Oe)	Remanence (%)
S1	195.5	1160	28
S2	186.3	905	30
S3	174.2	940	29
S4	189.3	853	22

The hysteresis loops measured up to 40 kOe at ambient temperature for samples S1, S2, S3, S4 are shown in Figures 5A, 5B, 5C, 5D, respectively. The results concerning saturation magnetization (M_s), coercivity (H_c) and remanence (R) are gathered in Table 1. Among all samples, the highest value of M_s was obtained for S1, prepared by nitridation of as prepared goethite at 140 °C, followed by S4 obtained by nitridation at 140 °C of goethite precursor crushed in mortar and processed in ultrasonic bath. Interestingly, H_c decreases strongly by processing the goethite precursor while M_s remained still relatively high and this behavior of H_c can be explained by deterioration of shape anisotropy during goethite processing. The sample S3 nitrided at 150 °C shows the lowest value of M_s . This value of M_s is expected, according to XRD and Mössbauer data for S3, due to the presence of important amounts of Fe_4N and metallic iron besides the main $Fe_{16}N_2$ phase. Also, the coercivity of sample S3 is lower than that of sample S1 due to the presence of Fe_4N and metallic iron phases with lower coercivity than $Fe_{16}N_2$ phase. However, the coercivity of S3 is higher than one of S4, even though the latter was nitrided at 140 °C and does not contain Fe_4N , suggesting that the deterioration of goethite precursor morphology has crucial influence on coercivity (which is directly correlated with shape anisotropy). The amount of $Fe_{16}N_2$ phase is the highest, according both to XRD and Mössbauer data, for S1 sample prepared at 140 °C from goethite precursor and this is in good agreement with the maximum value of M_s and H_c among all the samples. The sample S2 prepared at 140 °C from hematite precursor has lower M_s than S1 prepared at 140 °C from goethite precursor, which means that the penetration of ammonia into the hematite precursor is more difficult due to sticking of the particles which is also supported by the SEM images. This behaviour is well correlated with Mössbauer and diffraction data showing a higher amount of metallic iron in sample S2 compared with sample S1. Sample S2 coercivity is also lower than that of sample S1, proving that by nitridation of goethite it may be obtained a larger shape anisotropy compared with the one obtained by nitridation of hematite. However, by processing the goethite in mortar and ultrasonic bath, the coercivity decreases even more than for the sample obtained by nitridation of hematite.

Table 2. Hyperfine parameters: isomer shift (IS), quadrupole splitting (QS), hyperfine magnetic field (H), relative area (R.A.) for different crystallographic positions and phases and the ratios $Fe_{16}N_2/Fe$ measured from Mossbauer, respectively from XRD data for samples S1, S2, S3, S4

Sample	Phase	Pos.	IS(mm/s) ref. Fe met	QS(mm/s)	H (T)	R.A. (%)	$Fe_{16}N_2/Fe$ (Mossb.)	$Fe_{16}N_2/Fe$ (XRD)
S1	$Fe_{16}N_2$	4d	0.06(2)	-0.44(2)	29.60(3)	19.8(3)	9.7(5)	8.0(8)
		8h	0.18(2)	0.22(2)	31.53(3)	39.7(4)		
		4e	0.16(2)	-0.17(2)	40.18(3)	20.6(3)		
	oxide		0.38(2)	0.88(3)	-	11.7(2)		
	Bcc Fe		0.00	0.00	32.97(3)	8.2(3)		
S2	$Fe_{16}N_2$	4d	0.06(2)	-0.43(2)	29.55(3)	18.4(3)	5.2(3)	3.4(3)
		8h	0.18(2)	0.21(2)	31.52(3)	37.2(4)		
		4e	0.16(2)	-0.16(2)	40.15(3)	19.0(3)		
	oxide		0.36(2)	0.84(3)	-	11.1(2)		
	Bcc Fe		0.00	0.00	32.98(3)	14.3(3)		
S3	$Fe_{16}N_2$	4d	0.06(2)	-0.43(2)	29.52(3)	14.1(3)	3.7(2)	3.5(3)
		8h	0.18(2)	0.21(2)	31.41(3)	26.4(4)		
		4e	0.16(2)	-0.17(2)	40.15(3)	13.6(3)		
	oxide		0.40(2)	0.79(3)	-	11.1(2)		
	Bcc Fe		0.00	0.00	33.02(3)	14.5(3)		
	Fe_4N	1a	0.23(3)	0.02(3)	34.10(4)	5.1(2)		
		3c	0.31(3)	0.03(3)	21.91(4)	15.2(3)		
S4	$Fe_{16}N_2$	4d	0.06(2)	-0.44(2)	29.60(3)	18.9(2)	4.9(3)	5.5(4)
		8h	0.18(2)	0.21(2)	31.52(3)	37.0(3)		
		4e	0.16(2)	-0.17(2)	40.14(3)	19.4(2)		
	oxide		0.39(2)	0.86(3)	-	9.2(1)		
	Bcc Fe		0.00	0.00	33.01(3)	15.5(2)		

^{57}Fe Mössbauer spectroscopy is a powerful tool useful to analyze the electronic phenomena generated by various electron configurations which occur in iron containing compounds. Mössbauer spectra measured for samples S1, S2, S3, S4 at ambient temperature were presented in Fig. 6. The hyperfine parameters (isomer shift (IS), quadrupole splitting (QS), hyperfine magnetic field (H)) obtained by fitting the spectral components of the Mössbauer spectra from Fig. 6 are presented in Table 2. Together with magnetic measurements, Mössbauer spectra give information about the magnetic state. For example a ferromagnetic phase is characterized by a sextet (six-line pattern) while a paramagnetic phase is described by a doublet (2-line pattern). Usually, if the local environment of Fe in the paramagnetic phase is cubic the electric field gradient is zero and the doublet becomes singlet (one-line pattern).

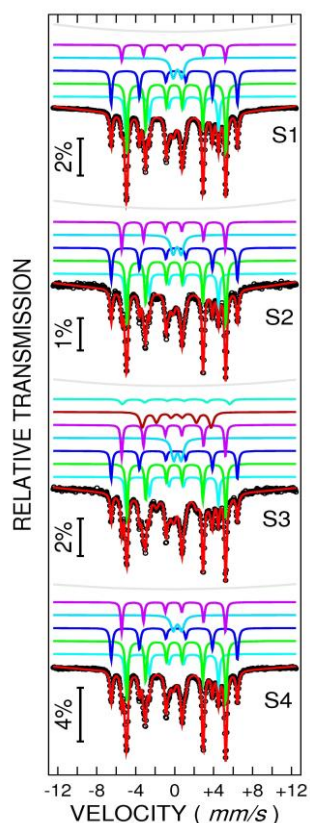


Fig. 6. Mössbauer spectra measured at ambient temperature for sample S1, S2, S3, S4 together with the fitted curve and the decomposition in spectral components

The Mössbauer spectrum gives a spectral component (sextet, doublet or singlet) for each non-equivalent crystallographic position. Consequently, the Mössbauer pattern will be an overlapping of spectral components (sextets, doublets and singlets) provided not only by various phases but also from different non-equivalent crystallographic positions belonging to the same phase. From the hyperfine parameters values of the spectral components can be obtained information about phase composition, valence and spin state, phase transitions, local distortion, etc. In contrast to the XRD patterns measured for powder samples, when only the non-amorphous phases can be well indexed, an amorphous phase containing iron is well evidenced in Mössbauer spectrum. The Mössbauer spectra presented in Fig. 6A – for sample S1, Fig. 6B – S2, Fig. 6D – S4 show only the presence of Fe_{16}N_2 , metallic iron and iron oxide. Additionally to these contributions, Mössbauer spectrum of sample S3 (Fig. 6C) exhibits also the presence of Fe_4N amorphous phase with broad lines. The line-widths for Fe_{16}N_2 and metallic iron are sharp for all samples. Fe_{16}N_2 phase is characterized by 3 non-equivalent positions: [4d], [8h] and [4e] with theoretical areas (given by the crystallographic occupancy for the perfect structure) in the ratio 1:2:1, respectively. However, due to the fact that iron occupancy in studied samples could deviate from the ideal one, we let the area ratio between the three non-equivalent positions to iterate during the fit. The obtained results are, within the error bars of the fit, close to the ideal 1:2:1 occupancy ratio (1:2:1 fitted relative area). The Mössbauer hyperfine fields corresponding to these positions given in literature vary: 39.5 T for Fe (4d), 31.2 T for Fe (8h), 30.1 T for Fe (4e) [21] and 40.4 T for Fe (4d), 31.6 T for Fe (8h), 29.8 T for Fe (4e) [12]. The values presented in Table 2 for the hyperfine parameters corresponding to all the three non-equivalent positions of Fe_{16}N_2 , about 40.15 T for Fe(4d), 31.52 T for Fe(8h), 29.6 T for Fe(4e) fit well between data previously presented in literature proving the reliability of our fits. Moreover, Mössbauer data presented in Table 2 show also the IS and QS values for Fe(4d), Fe(8h) and Fe(4e) non-equivalent positions which are in good agreement with the values from literature [21]. Additionally to Fe_{16}N_2 phase, in the

Mössbauer patterns of all samples can be evidenced a central broad doublet with isomer shift (IS) of about 0.38 mm/s (referred to metallic iron) and quadrupole splitting (QS) of about 0.83 mm/s specific to superparamagnetic iron oxide. Low temperature measurements reported elsewhere by the authors show the transformation of the doublet from ambient temperature into a sextet at 5 K with hyperfine magnetic field specific to superparamagnetic small particles containing defected magnetite/maghemite. The third phase which occurs in all samples is metallic iron, with a hyperfine magnetic field of about 33 T at ambient temperature. Besides Fe_{16}N_2 , metallic iron and iron oxide structures, the only sample which has additional phase (Fe_4N) revealed both in XRD and Mössbauer pattern is sample S3 (obtained by nitridation at 150 °C of goethite). The Mossbauer pattern corresponding to Fe_4N phase shows two positions with hyperfine fields of 21.9 T and 34.1 T and occupancy ratio 3:1, respectively. It seems that increasing the temperature above 140 °C is not useful in order to obtain Fe_{16}N_2 samples with high purity and good magnetic properties because above this temperature starts the precipitation of Fe_4N . The relative areas corresponding to the iron amount contained in various phases and distributed over the three non-equivalent positions of Fe_{16}N_2 are also presented in Table 2. Moreover, in the same table is presented the ratio between the amount of iron contained in Fe_{16}N_2 and that one contained in metallic iron as obtained from Mössbauer data. Also, Table 2 indicates the same ratio calculated from XRD data as the ratio between the weighted areas of the peaks belonging to the (422) reflection for Fe_{16}N_2 ($2\Theta = 81.106^\circ$) and (211) reflection for metallic iron ($2\Theta = 82.335^\circ$) as described before at the section corresponding to the interpretation of diffraction data. There is a pretty good agreement between the ratios obtained from XRD data and that obtained from Mössbauer relative areas, at least for the samples obtained using goethite precursor, taking into account the errors for determinations of this ratio from XRD data where the peaks of interest have small relative intensity and consequently high statistical noise. Most probable, the metallic iron cores are surrounded by Fe_{16}N_2 shells due to the impossibility of ammonia to penetrate deep in the metallic iron particles obtained from goethite at these low temperatures. The location of iron oxides in these samples is partially in small superparamagnetic particles and partially at the external face of Fe_{16}N_2 shell/Fe core particles keeping in mind that we processed the particles in air during XRD and Mössbauer measurements. Using the relative area of various iron containing phases from Table 2 and the M_s values from Table 1 we obtained a good matching between experimental and simulated data considering for Fe_{16}N_2 phase a value $M_s=226$ emu/g, for metallic iron phase $M_s=198$ emu/g and for superparamagnetic iron oxide particles a value $M_s= 24$ emu/g. The value obtained for Fe_{16}N_2 phase is close to the value obtained by Ogawa et al. [22] at ambient temperature and clearly indicates that Fe_{16}N_2 has giant saturation magnetization, higher than one of metallic iron particles with similar dimensions and morphology [23]. Also the coercivity of obtained Fe_{16}N_2 particles (among all samples the highest H_c was 1160 Oe) is higher than that corresponding to metallic iron particles (H_c about 400 Oe) with similar characteristics [23].

Conclusions

Goethite particles with acicular shape and diameters of about 100 nm and lengths of 2000 nm were successfully used for the preparation of Fe_{16}N_2 particles, maintaining their acicular shape after reduction and nitridation processing. For the best sample, the amount of Fe_{16}N_2 phase is higher than 81 %, while about 11 % is iron oxide due to sample manipulation in air and about 8% is un-reacted iron due to the difficulty of ammonia to penetrate deep in metallic iron particles at temperatures below 200 °C. By nitridation at about 150 °C, Fe_4N phase begins to form, its presence implying the deterioration of magnetic properties. The samples prepared by goethite nitridation have better magnetic properties compared to those obtained by nitridation of hematite. The ratios between the $\text{Fe}_{16}\text{N}_2/\text{Fe}$ amounts as resulted from Mössbauer and XRD data are in good agreement. Using magnetic and Mössbauer data we estimated that Fe_{16}N_2 prepared according to our method has $M_s=226$ emu/g at ambient temperature, higher than that of metallic iron.

Acknowledgements

This work was realized through the program Partnership in priority areas PN II developed with the support of MEN - UEFISCDI, project PN-II-PT-PCCA-2013 (project contract no. 275/2014). The technical support of Gheorghe Gheorghe and Aurel Leca is strongly acknowledged.

References

- [1] K.H. Jack, Proc. R. Soc. London Ser. A **208**, 214 (1951).
- [2] T. K. Kim, M. Takahashi, Appl. Phys. Lett. **20**, 492 (1972).
- [3] M. Komuro, Y. Kozono, M. Hanazono, Y. Sugita, J. Appl. Phys. **67**, 5126 (1990).
- [4] M. Takahashi, H. Shoji, H. Takahashi, H. Takahashi, T. Wakiyama, M. Kinoshita, W. Ohta, IEEE. Trans. Magn. **29**, 3040 (1993).
- [5] K. Nakajima, S. Okamoto, Appl. Phys. Lett. **56**, 92 (1990).
- [6] H. Y. Wang, Z. W. Ma, E. Y. Jiang, Y. J. He, H. S. Huang, Appl. Phys. A **68**, 559 (1999).
- [7] S. Atiq, H. -S. Ko, S. A. Siddiqi, S. -C. Shin, J. Alloy Compd. **479**, 755 (2009).
- [8] A. Tayal, M. Gupta, A. Gupta, M. Horisberger, J. Stahn, Thin Solid Films **536**, 39 (2013).
- [9] H. Tanaka, H. Harima, T. Yamamoto, H. Katayama-Yoshida, Y. Nakata, Y. Hirotsu, Phys. Rev. B **62**(22), 15042 (2000).
- [10] H. Sims, W.H. Butler, M. Richter, K. Koepernik, E. Aşloğlu, C. Friedrich, S. Blügel, Phys. Rev. B **86**(17), 174422 (2012).
- [11] A. Nagatomi, S. Kikkawa, T. Hinomura, S. Nasu, F. Kanamaru, J. Jpn. Soc. Powder Powder Metal. **46**(2), 151 (1999).
- [12] S. Kikkawa, A. Yamada, Y. Masubuchi, T. Takeda, Mater. Res. Bull. **43**, 3352 (2008).
- [13] S. Kikkawa, K. Kubota, T. Takeda, J. Alloy Compd. **449**, 7 (2008).
- [14] K. Yamanaka, Y. Onuma, S. Yamashita, Y. Masubuchi, T. Takeda, S. Kikkawa, J. Solid State Chem. **183**, 2236 (2010).
- [15] S. Yamashita, Y. Masubuchi, Y. Nakazawa, T. Okayama, M. Tsuchiya, S. Kikkawa, J. Solid State Chem. **194**, 76 (2012).
- [16] Y. Masubuchi, H. Sato, T. Motohashi, S. Kikkawa, J. Ceram. Soc. of Japan **122**(4), 288 (2014).
- [17] D. Nagai, Y. Kinemuchi, K. Suzuki, A. Towata, M. Yasuoka, J. Solid State Chem. **225**, 455 (2015).
- [18] K. Takagi, M. Akada, K. Ozaki, N. Kobayashi, T. Ogawa, Y. Ogata, M. Takahashi, J. Appl. Phys. **115**(10), 103905 (2014).
- [19] A. M. Cojocariu, A. Doaga, W. Amin, P. Bender, R. Hempelmann, O. F. Caltun, Dig. J. Nanomater. Bios. , **8**(2), 519 (2013).
- [20] C. Jin, Z. Haiyan, L. Liping, Z. Li, Dig. J. Nanomater. Bios. , **8**(1), 43 (2013).
- [21] Q. Qi, K. O'Donnell, E. Touchais, J.M.D. Coey, Hyp. Inter. **94**, 2067 (1994).
- [22] T. Ogawa, Y. Ogata, R. Gallage, N. Kobayashi, N. Hayashi, Y. Kusano, S. Yamamoto, K. Kohara, M. Doi, M. Takano, M. Takahashi, Appl. Phys. Express, **6**(7), 073007 (2013).
- [23] J. Mendez-Garza, B. Wang, A. Madeira, C. Di Giorgio, G. Bossis, J. Biomat. and Nanobio. **4**(3), 222 (2013).